Stat3 controls cell death during mammary gland involution by regulating uptake of milk fat globules and lysosomal membrane permeabilization

Timothy J. Sargeant[#1], **Bethan Lloyd-Lewis**[#1], **Henrike K. Resemann**[1], **Antonio Ramos-Montoya**[2], **Jeremy Skepper**[3], and **Christine J. Watson**[1,5]

[1]Department of Pathology, University of Cambridge, Tennis Court Road, Cambridge CB2 1QP, UK

[2]Uro-Oncology Research Group, CRUK Cambridge Institute, University of Cambridge, Li Ka Shing Centre, Robinson Way, CB2 0RE, UK

[3]Department of Physiology, Development and Neuroscience, University of Cambridge, Tennis Court Road, Cambridge CB2 1QP, UK

[#] These authors contributed equally to this work.

Abstract

We have previously demonstrated that Stat3 regulates lysosomal mediated-programmed cell death (LM-PCD) during mouse mammary gland involution *in vivo.* However, the mechanism that controls the release of lysosomal cathepsins to initiate cell death in this context has not been elucidated. We show here that Stat3 regulates the formation of large lysosomal vacuoles that contain triglyceride. Furthermore, we demonstrate that milk fat globules (MFGs) are toxic to epithelial cells and that, when applied to purified lysosomes, the MFG hydrolysate oleic acid potently induces lysosomal leakiness. Additionally, uptake of secreted MFGs coated in butyrophilin 1A1 is diminished in Stat3 ablated mammary glands while loss of the phagocytosis bridging molecule MFG-E8 results in reduced leakage of cathepsins *in vivo*. We propose that Stat3 regulates LM-PCD in mouse mammary gland by switching cellular function from secretion to uptake of MFGs. Thereafter, perturbation of lysosomal vesicle membranes by high levels of free fatty acids results in controlled leakage of cathepsins culminating in cell death.

INTRODUCTION

Lysosomes are key eukaryotic organelles that are essential for the turnover of cellular macromolecules and organelles that are delivered via the endocytic, autophagic and phagocytic membrane trafficking pathways[1]. Whilst previously considered simply as the final destination for cargo intended for breakdown it is becoming increasingly apparent that lysosomes, and their acid hydrolase contents, possess many other specific functions. Notably, this includes the initiation or enhancement of cell death programmes as a result of permeabilisation of lysosomal membranes and the subsequent leakage of cathepsins and other constituents into the cytosol, where they can act as executioner proteases[1-3]. Aberrant lysosomal function is associated with ageing and neurodegenerative disorders such as Parkinson's disease and lysosomal storage disorders[4, 5]. Furthermore, cellular transformation is characterised by lysosomal modifications, including changes to their size, localisation and composition and enhanced secretion of their contents to the extracellular space, promoting tumour progression, invasion and metastasis[6-8]. Conversely, apoptosis or lysosomal-mediated cell death can be induced by the intracellular release of lysosomal hydrolases, providing a rationale for utilising anti-cancer drugs that destabilise lysosomal membranes[7, 9].

An exquisite example of controlled physiological cell death is the post-lactational regression (involution) of the mammary gland, one of the major cell death events to occur in the adult mammalian organism[10,11]. During pregnancy, alveolar epithelial progenitor cells are stimulated to proliferate and differentiate in response to progesterone and prolactin in order to provide mammary tissue with the secretory cells necessary for milk production during lactation[12]. This includes secretion of milk proteins as well as MFGs via a unique mechanism that requires butyrophilin 1A1 (BTN) and xanthine dehydrogenase/ oxidoreductase (XDH)[13]. A complex and highly regulated programme of cell death and tissue remodelling is initiated upon cessation of lactation to remove alveolar mammary epithelium and return the gland to its pre-pregnant state[11]. This process occurs in two phases, with the first phase (0-48h in the mouse) being reversible such that re-introduction of the pups can re-initiate lactation[14]. Prolactin-induced Stat5 signalling is abrogated, and LIF-induced Stat3 signalling is initiated, upon induction of involution. Stat3 is indispensable for this process as mice with a mammary epithelial-specific knockout of Stat3 display diminished cell death and a severe delay in post-lactational regression of the gland[15, 16].

We have shown previously that cell death in the regressing mammary gland occurs independently of caspases, relying instead on lysosomal membrane permeabilisation (LMP) and the release of cathepsin proteases to the cytosol[17]. Intriguingly, this mode of cell death is unlikely to be restricted to the mammary gland. Cell death during hormonoprivic involution of the prostate gland[18] and in the labial gland of the tobacco hornworm, bear striking similarities to LM-PCD in mammary epithelial cells during involution[19]. Stat3 regulates this process by stimulating the expression of cathepsins B and L, in addition to concurrently suppressing expression of the endogenous cathepsin inhibitor, Spi2A[17]. This latter event leaves mammary epithelial cells particularly susceptible to cell death from the amplified activity of cathepsins that have leaked from lysosomal structures. A role for LMP

in mediating a physiological cell death program, rather than in pathological conditions or as a back-up mechanism for refractory apoptosis had not been previously described[20].

A number of mechanisms have been proposed for LMP in different cellular contexts *in vitro* including lysosomotropic detergents, toxins, reactive oxygen species, and translocation of Bax to the lysosomal membrane[21-23]. However, a definitive mechanism driving LMP *in vivo*, and the specific role of Stat3 in this process, has yet to be elucidated. We hypothesised that Stat3 drives a series of biological events in the regressing mammary gland that amplifies the lysosomal system at a time of increased demand and stress, while concurrently exploiting this to mediate lysosomal-dependent cell death. We have explored this notion by investigating the micro-architecture of mammary epithelial cells in lactating and involuting mammary glands and discovered that Stat3 mediates the formation and fusion of large lysosomal-like vacuoles many of which contain triglyceride. This is subsequently metabolised to free fatty acids, including oleic acid, that can distort membranes and result in leakage of cathepsins from lysosomes. We also reveal that Stat3 promotes a phenotypic switch from secretion to phagocytosis of MFGs, the latter function delivering triglyceride to vacuoles with the ensuing consequences of LMP and cell death.

Results

Large vacuolar structures appear during involution

Our initial approach to investigate the hypothesis that Stat3 both enhances, and exploits, the lysosomal system to mediate cell death was to examine the lysosomal compartment during mammary gland regression in more detail. We noted the appearance of large cathepsin D-positive vacuoles upon initiation of involution (Fig. 1a). Significantly, similar vacuoles also appear upon induction of involution in the uterus and prostate (Fig. 1a), and were often larger than nuclei (> 5 μm). Importantly, such a dramatic increase in size is a factor that could, of itself, sensitise lysosomes to become leaky[24]. Notably, the morphology of dead cells in all three tissues was similar, being atypical for either classical apoptosis or necrosis (Fig. 1b), and characterised by hypercondensed nuclei and a complete absence of membrane blebbing[18]. This suggests a common mechanism of cell death during regression of hormone-dependent tissues.

We then focussed our studies on these presumptive lysosomal vesicles in the regressing mammary gland. Cathepsin D is co-ordinately upregulated with cathepsins B and L at 24-48h involution (Supplementary Fig. 1a, b) and [17, 25, 26], with large cathepsin D structures also staining positively for the lysosomal membrane marker, LAMP2 (Fig. 1c). Several very large LAMP2-positive lysosomal vacuoles were frequently seen within individual epithelial cells in the involuting, but not the lactating, mammary gland (Fig. 1d). These structures were much less apparent in tissue from *Stat3^fl/fl;BLG-Cre* (Stat3 knockout) mice that are specifically deleted for Stat3 in the luminal epithelium, compared to *Stat3^fl/fl* control mice (Fig. 1e). Quantification of the number of LAMP2-positive structures per nucleus showed a 9-fold decrease in the Stat3 knockout epithelium (Fig. 1f). This effect was observed only during the first phase of involution. At 48 h and 72 h involution, Stat3 ablation had a diminished effect on the presence of lysosomal vacuoles (Supplementary Fig. 1c), although expression of cathepsins B and L is dramatically reduced at these timepoints in Stat3

knockout glands[17]. Upon further characterisation, triglyceride lipid was found to be a significant constituent of the lysosomal system in involuting mammary gland (Fig. 1g and Supplementary Fig. 1d). Thus, these large structures contain lysosomal proteins and triglyceride showing that fusion of lysosomes with either unsecreted or re-absorbed MFGs has taken place.

Ultrastructural analysis of vacuoles and their contents

In order to analyse these structures in greater detail, we performed transmission electron microscopy (TEM) on perfusion fixed mammary tissue from day10 lactation and 24h involution. This revealed the presence of strikingly large, membrane-bound vesicles, many of which were at least the size of nuclei with some occupying most of the cell (Fig. 2a). These have been observed also by TEM at day 3 involution[27]. Notably, these were present only during involution and not at day10 lactation (Fig. 2a). Once again, in agreement with our observations on LAMP2-positive vacuoles, these large vacuoles were much less abundant in Stat3 knockout tissue (Fig. 2a). Additionally, we noted that mitochondria acquire an elongated morphology upon the switch from lactation to involution that occurred regardless of Stat3 status (Fig. 2a). This has previously been described as an adaptive response to a highly autophagic environment[28]. The presence of morphologically sound mitochondria, which appeared similar in both control and Stat3 deficient mammary tissue at 24h involution, further supports our previous data showing that cell death at this time is caspase independent[17]. Confirming results in Figure 1a and c, immunogold staining for cathepsin D showed this lysosomal enzyme to be focally associated with degrading material contained within vacuoles (Fig. 2b), revealing their lysosomal origin. Vacuoles containing autophagic contents (Fig. 2c), milk protein (Fid. 2d, e) and triglyceride (Fig. 2 f-i) were frequently observed to be in the process of fusion with other membrane bound structures (Fig. 2c, e and f), clearly demonstrating an active process of vesicle biogenesis. Furthermore, lipid was observed inside lysosomal structures that also contained electron-dense lipofuscin-like material (Fig. 2h, i), confirming hydrolysis of bulk triglyceride from lipid droplets in the lysosomal compartment.

Vesicles are induced by Stat3 in mammary epithelial cells *in vitro*

Intrigued by the association of large lysosomal vacuoles with the initiation of cell death, and their absence in the Stat3 knockout, we sought to determine a mechanistic involvement of these structures in the execution of cell death. To address this question, we utilised oncostatin M (OSM) stimulation of the EpH4 mammary epithelial cell line, which we have previously shown to mimic Stat3-induced LM-PCD[17]. We observed a number of vacuoles/vesicles in unstimulated EpH4 cells presumably generated by autophagy and by pinocytosis of the culture medium (Fig. 3a). We then determined whether activation of Stat3 by OSM resulted in a stimulation of the biogenesis of such vesicles. This was indeed the case with OSM treatment resulting in a 1.7-fold increase in the volume fraction of degradative vesicles after 72 h treatment as determined by TEM (Fig. 3 b-d).

Milk-derived lipid and fatty acids are toxic to mammary epithelial cells

Having confirmed that EpH4 cells can take up substances from the culture medium we incubated cells with freshly collected mouse milk which resulted in lipid accumulation (Fig.

4a) and induction of cell death, as measured by phase contrast microscopy (Fig. 4a) and cell viability analysis (Fig. 4b).

Immunofluorescence imaging of milk-fed EpH4 cells revealed lipid localising to lysosomal compartments (Supplementary Fig. 2a), while co-treating with Bafilomycin A1, a potent and selective inhibitor of the vacuolar-type H+ ATPase [29] that inhibits lysosomal acidification and vesicular fusion, resulted in a partial rescue of milk-induced cytotoxicity (Fig. 4c,d), suggesting that lysosomal lipid accumulation induces cell death.

The toxicity of milk could be due to several components as it contains protein, triglyceride, carbohydrates, minerals and antibodies. Triglycerides are the primary constituent of MFGs [30] that are degraded in the lysosome during involution, yielding potentially high local concentrations of free fatty acids. Thin layer chromatography (TLC) analysis (Fig. 4e) revealed that free fatty acids are present in the mammary gland during involution, but are not detectable during lactation. Free fatty acid concentration as measured by TLC, using oleic acid standards, averaged 4.8 μg/20mg tissue (Fig. 4f,g), which corresponds to a tissue level of approximately 850 μM free fatty acid (see Methods). It should be noted that only unsaturated free fatty acid could be detected using this system implying that 850 μM is a conservative estimate.

The fatty acids found in milk triglycerides are summarised in Supplementary Table 1, with oleic ($CH_3(CH_2)_7CH=CH(CH_2)_7CO_2H$) and palmitic ($CH_3(CH_2)_{14}CO_2H$) acids being the most abundant[31] and hence chosen for further analysis in vitro. Stearic acid ($CH_3(CH_2)_{16}CO_2H$) was also used, as it has the same number of carbon atoms as oleic acid but lacks the double bond.

The role of free fatty acids in lysosome permeabilisation and cell death was then investigated using EpH4 cells. Treatment with physiological levels of oleic and palmitic acids (as determined in Fig. 4e-g) resulted in lipid accumulation and toxicity, as observed by phase contrast microscopy and cell viability analysis (Fig. 4h,i and, Supplementary Fig. 2b,c). Notably, oleic acid treatment resulted in more staining for triglyceride than palmitic acid. Stearic acid treatment resulted in less lipid accumulation, but no cytotoxicity was observed at equivalent concentrations to oleic and palmitic acids (Figure 4i). The ability of oleic acid to elicit more triglyceride synthesis is well documented[32] and is considered a protective mechanism from the toxic effects of oleic acid exposure.

Cathepsin activity assays and immunoblot analysis on digitonin-extracted cytosolic fractions (optimised for digitonin concentration to avoid damage to lysosomes; Supplementary Fig. 3a) of fatty acid treated EpH4 cells revealed that oleic acid caused a significant release of cathepsins to the cytosol (Fig. 5a). Immunoblot analysis of these samples further demonstrated that only oleic acid induces significant release of cathepsin L to the cytosol (Fig. 5b). In contrast, palmitic acid treatment resulted in limited release of cathepsins to the cytosol, which was not significant. Importantly stearic acid, the saturated carbon chain counterpart of oleic acid, also had no effect on cathepsin release as measured by cytosolic cathepsin activity assays and immunoblot (Fig. 5a,b). Staining with the lysosomotropic dye LysoTracker® Red showed that both oleic and palmitic acid treatment resulted in an

appearance of a population of cells with low Lysotracker® intensities, indicative of lysosomal de-acidification (Supplementary Fig. 3b,c). Of note, fatty acid treatment did not appear to induce the translocation of the pore-forming protein Bax to lysosomes in EpH4 cells (Supplementary Fig. 4). Therefore, these data clearly demonstrate that lysosomal membranes can be permeabilised efficiently by oleic acid. However, an effect of palmitic acid cannot be completely excluded.

Oleic acid treatment permeabilises purified lysosomes

It has been observed that palmitic, but not oleic acid, induces cell death by ROS-mediated mitochondrial disruption[33]. In order to exclude potential indirect effects such as mitochondrial ROS-induced perturbations upstream of lysosomal permeability[34] we isolated lysosomes from EpH4 cells using a magnetic nanoparticle separation protocol (Fig. 5c), which produces pure lysosomal preparations uncontaminated by mitochondria (Fig. 5d). Addition of fatty acids to purified lysosomes for up to 30 mins followed by immunoblot analysis showed leakage of cathepsin L in the presence of oleic acid while lysosomes were essentially intact in the presence of palmitic acid (Fig. 5e). Thus, oleic acid is a potent lysosomal permeabilisation agent at concentrations below that present locally in the mammary gland during involution, whilst palmitic acid is unable to permeabilise membranes within the timeframe studied. Oleic acid possesses an unsaturated cis-bond and adopts a kinked conformation which has been shown to distort synthetic membranes and leads to their de-stabilisation upon insertion[35] (Fig. 5f). In contrast, palmitic and stearic acid are linear in conformation as they lack a double bond. Thus, the increased potency of oleic acid is likely to be due to the kink in its structure. The oleic acid-bovine α-lactalbumin complex, BAMLET, has been hypothesized to cause LM-PCD by interaction with the lysosomal membrane[36]. However, it has since emerged that cell death caused by BAMLET, and its human counterpart HAMLET, is due solely to the function of α-lactalbumin as a carrier for oleic acid[37]. Our data support this observation and emphasise the potency of oleic acid as a phospholipid membrane destabiliser. Since this leak of cathepsins mimics our observations in vivo[17], we suggest that insertion of MFG-derived fatty acids, and in particular oleic acid, into the limiting membrane of these lysosomal vesicles produces membrane distortions resulting in leakage of cathepsins into the cytosol. This posit is further supported by the slow leak of cathepsins[17] and the essentially intact lysosomal/vacuolar membranes observed during involution *in vivo* (Fig. 2).

Stat3 mediates uptake of BTN-coated MFGs

In the process of being secreted, MFGs become coated with BTN, which is essential for their secretion[38]. BTN can be visualised as a thin ring surrounding MFGs secreted into the alveolar lumen at day 10 lactation (Fig. 6a). Notably, unsecreted lipid droplets within the mammary epithelium do not stain for BTN[38]. At 24 h involution, the appearance of MFGs coated with BTN becomes strikingly evident within the mammary epithelium (Fig. 6a). This is Stat3 dependent as considerably fewer MFGs coated with BTN are evident in Stat3^{fl/fl};BLG-Cre glands at 24 h involution (Fig. 6b) indicating reduced uptake of MFGs. Interestingly, microarray analysis indicates that expression of BTN and XDH is suppressed at the onset of involution (Fig. 6c) and [39] (www.path.cam.ac.uk/~madgroup). Quantitative PCR analysis shows these genes are upregulated in Stat3 KO mammary gland at 24 h

involution, suggesting Stat3 represses XDH and BTN transcription (Supplementary Table 2). Immunoblot of Stat3 knockout and control mammary tissue corroborates the role of Stat3 in suppressing BTN expression (Fig. 6d).

MFGs are taken up by mammary epithelial cells via phagocytosis

Having firmly established the presence of triglyceride lipid in secondary lysosomes, we sought to define how lipid was trafficked to these large lysosomal vacuoles. Intracellular lipid can be delivered to the lysosome via macroautophagy (lipophagy)[40]. However, having shown that BTN-coated secreted lipid droplets were being taken up by the alveolar epithelium, we looked for further evidence of endocytic uptake.

As demonstrated by BTN staining in Figure 6, MFGs observed in the alveolar lumen with TEM are surrounded by a thin rim of plasma membrane-encased cytosol and the MFG membrane (Fig. 7a). This latter structure is acquired by the lipid droplet during the secretion process from the apical surface of the epithelium[13] and is direct evidence that intracellular lipid droplets are taken up by an endocytic pathway. Indication of macropinocytosis is seen at the plasmalemma, where membranous ruffles capture luminal fluid (Fig. 7b). In agreement with this, macropinosomes, some containing lipid droplets, are seen within the epithelium (Fig. 7c). However, large MFGs that have come from the alveolar lumen are also taken up by phagocytosis. MFGs are seen inside tightly fitting phagosomes within the epithelium (Fig. 7d-f). The luminal origin of fat droplets (that can measure 8 μm in diameter) is confirmed by the presence of the MFG membrane that is found in close proximity to the limiting phagosomal membrane (Fig. 7f). The highly phagocytic nature of involuting mammary gland epithelium is seen clearly in cathepsin L knockout mice that, in contrast to control animals, cannot efficiently degrade cell corpses within the phagolysosome, thereby allowing visualisation of phagocytosed material (Fig. 7g). Further support that mammary epithelial cells become phagocytes[41] comes from expression of the recognition molecule CD14, on the luminal surface in a Stat3 dependent manner at 24 h involution[42]. These data unequivocally demonstrate that mammary epithelial cells become phagocytes during involution and thus deliver MFGs to lysosomes.

Delivery of MFGs by phagocytosis would traffic MFGs to lysosomes for hydrolysis and generation of toxic free fatty acids[43]. In support of this contention, knockout of the phagocytosis bridging molecule MFG-E8 slows mammary gland involution[44, 45]. MFG-E8 staining is clearly visible on MFGs and dead cells within the alveolar lumen during involution (Fig. 7h). As expected, luminal MFG-E8 staining is abolished in MFG-E8 knockout tissue (Fig. 7h) and corresponds with decreased leakage of cathepsin proteases from lysosomes at 24 h involution as measured by cytosolic cathepsin activity (Figure 7i). This strongly suggests that phagocytosis of MGFs by viable epithelium results in lysosomal damage.

Thus, we propose a model for Stat3 mediated cell death during involution, which encompasses this switch in mammary epithelial phenotype from a secretory cell to non-professional phagocyte (Fig. 8). To embrace this role, Stat3 powerfully enhances the lysosomal system while at the same time suppressing expression of the protective cytosolic protease inhibitor Spi2a. Uptake of triglyceride and delivery to lysosomes, with subsequent

production of fatty acids, results in permeabilisation of large lysosomal vacuoles. The consequent leakage of cathepsin proteases into the cytosol is the final fatal step that causes physiological LM-PCD in the involuting mammary gland (Fig. 8).

Discussion

Cell death during involution of the mammary gland is a genetically controlled process that is both dramatic in scope and efficient in execution. Although assumed to be an apoptotic process, our previous work suggested a non-apoptotic mechanism that required both Stat3 and leakage of cathepsins from lysosomes through lysosomal membrane permeabilisation (LMP)[17]. Many mechanisms of LMP in different cell types have been described *in vitro*, often with conflicting results and no consensus has been reached. We have thus focused on deciphering the mechanism of LMP in the *in vivo* context of mammary gland involution where cell death is a developmentally regulated physiological process.

Upon examination of involuting mammary tissue, we noted the association of cell death with the formation and fusion of large cytosolic vacuoles, many of which contained triglyceride, milk protein and degraded membranes. Furthermore, the appearance of these vacuoles requires Stat3, suggesting that this is a transcriptionally regulated event. Importantly, we show here that involution of other tissues such as prostate and uterus is characterised by similar histological hallmarks suggesting that formation of vacuoles and their fusion with lysosomes, leading to leakage of their cathepsin protease contents, could be a conserved mechanism of developmental cell death in hormone-dependent tissues.

The presence of vacuoles has previously been described in some forms of caspase-independent cell death in a variety of organisms. One of the earliest descriptions is of cells dying during metamorphosis of insect intersegmental muscle cells[46]. The role of vacuoles in plant cell death, during the formation and elimination of tissue, is well established and is associated with release of hydrolases from collapsed lytic vacuoles[47, 48], while vacuolisation is a prominent feature of dying *Dictyostelium discoideum* cells[49]. More recently, an activated form of the H-Ras oncoprotein was shown to induce extensive vacuolisation by macropinocytosis with subsequent cell death in cultured carcinoma cells. This process was named methuosis[50]. Furthermore, a small molecule named Vacquinol-1 was shown to induce catastrophic vacuolisation in glioblastoma cells[51] highlighting the utility of such an approach for killing apoptosis-resistant cancers.

Interestingly, while vacuolisation of itself can kill, delivery of triglyceride to lysosomes accelerates this process. EpH4 mammary epithelial cells die 72 h after the induction of extensive vacuolisation, whilst the addition of milk to these cells can induce cell death within 24 h. *In vivo*, dying mammary cells are shed into the alveolar lumen within 12 h of milk stasis and extensive cell death is apparent by 24 h involution. Thus, we suggest that the genetic control of vacuolisation, coupled with regulated uptake of triglyceride, is a potent inducer of cell death in mammary tissue. Furthermore, many diseases such as non-alcoholic liver disease, obesity and diabetes are characterised by cellular uptake of lipid[52]. Thus, this mechanism of cell death may be utilised more widely.

This work delineates a fundamental mechanism for LMP *in vivo.* The role of vacuolisation in this process is intriguing and may signify that the late evolving mammary gland has hijacked an ancient mechanism embraced by social amoebae and the plant kingdom for regulated cell death. Lastly, changes to the lysosomal compartment during mammary gland involution are reminiscent of changes in cancer cells, many of which are refractory to apoptosis and frequently harbour constitutively active Stat3[53]. Thus understanding the mechanism of LMP, and the critical role of Stat3 in this process, will provide new approaches to cancer therapy.

Methods Summary

Animal Husbandry

C57BL/6J wild-type mice were used for lipidtox stained sections, lipid analysis by TLC and in electron microscopy experiments. Stat3^{fl/fl} (control) or Stat3^{fl/fl};BLG-Cre (Stat3 knockout) mice are on a mixed background and were generated by crossing mice carrying *loxP* flanked *stat3*[54] with mice containing a β-lactoglobulin-promoter-driven Cre gene[55]. Other mouse strains used were cathepsin L knockout mice[56] and MFG-E8 knockout mice expressing a β-galactosidase-containing fusion protein under the control of the endogenous *Mfge8* promoter[57] (both strains on a C57L/6J background). Prostate sections were taken from NOD scid gamma mice (males aged between 4-6 months). Uterus samples were from 129 (involuting) or MF1 (control) background strain female mice that were between 4-6 months old. The mice were bred in regular IVC cages with food and water *ad libitum* and environmental enrichment. For mammary gland studies, virgin female mice between the ages of 7-10 weeks old were mated and males subsequently removed before birth to avoid second pregnancies. For involution studies, pups were removed at 10 days of lactation and dams killed at indicated time points. At least three mice were used for each time point in every experiment, with precise numbers indicated in figure legends. Animals were randomised between the groups and within cohorts of the same genotype. No statistical method was used to determine predetermine sample size. The investigators were blinded where possible, including the histological counting undertaken for Figure 6b. All animal experimentation was carried out in accordance with Animal (Scientific Procedures) Act 1986 and local ethical committee approval. Mice were sacrificed by dislocation of the neck, or terminal anaesthesia for TEM analysis.

Cell culture

EpH4 cells[58] were maintained in DMEM (Life Technologies) media supplemented with 10% FCS (Sigma) at 37 °C in a humidified atmosphere of 5% CO_2. Milk collected from 24 h involuting mammary glands was incubated on cells diluted to 10% in media. 400 μl was used in a 4 cm^2 well. Fatty acids purchased from Sigma-Aldrich (stearate, S3381, palmitate, P9767 and oleate O7501) were dissolved in ethanol and used at concentrations indicated in figure legends. Cells were treated with milk and fatty acids for 8 h or overnight as indicated. Cytotoxicity was assessed by trypan blue exclusion. For OSM stimulation cells were stimulated at 50% confluency with a final concentration of 25 ng ml^{-1} recombinant mouse Oncostatin M (495-MO, R&D Systems) or carrier (0.0001% BSA in PBS). Medium was

renewed every 48 h. Cells were pre-treated with 200nM Bafilomycin A1 (Sigma) for 1 h prior to milk addition for further 8 h.

Immunohistochemistry

For histological analysis on paraffin embedded tissues, abdominal glands were fixed in 4% formaldehyde in PBS overnight at room temperature. Glands were transferred to 70% ethanol and stored at −20 °C until embedding in wax and sectioned at 5 µm. Perfuse-fixed glands were embedded in wax or OCT for cryo-sections. Paraffin-embedded sections were de-paraffinized in xylene, and antigen retrieval performed by boiling in 10 mM Tri-sodium citrate buffer, pH 6.0, for 10 min. Sections were blocked in 10% goat serum (Sigma) in PBS, or normal chick serum (Sigma) in the case of Cathepsin D, for 1 h at room temperature. Sections were incubated with primary antibody overnight at 4 °C. Primary antibodies used were: rat anti-LAMP2 (ab13524, Abcam 1:50), rabbit anti-E-cadherin (#3195s, Cell Signalling Technologies, 1:200), goat anti-cathepsin D (AF1029, R&D Systems, 1:200), rabbit anti-BTN 1A1 (a generous gift from Dr Ian Mather, 1:5000) and armenian hamster anti-MFGE8 (clone 18A2, a generous gift). Secondary antibodies used were Alexa Fluor 488 goat anti-rabbit IgG (Life Technologies; 1 : 500) Cy3 goat anti-rat IgG (Life Technologies; 1 : 500) and Cy3 chicken anti-goat IgG (Life Technologies; 1 : 500). Lipidtox (H34475, Life Technologies) staining in vivo was performed on perfuse-fixed, cryosectioned tissues at 1:200. Nuclei were counterstained with Hoechst 33342 (Sigma Aldrich; 1 : 1000).

For tissue-culture samples, EpH4 cells were seeded on glass coverslips. Cells were fixed with 4% paraformaldehyde for 10 min, permeabilized with 0.1% saponin in PBS for 10 min and blocked in 10% normal goat serum (Sigma) in PBS, 0.01% saponin for 1 h at room temperature. Cells were incubated with primary antibody in 10% normal goat serum and 0.01% saponin in PBS overnight at 4 °C. Primary antibodies used were rat anti-LAMP2 (ab13524, Abcam 1:200) and rabbit anti-AIF (#4642s, Cell Signalling Technologies, 1:100). Fluorescent secondary antibodies and nuclei visualisation was as above for tissue sections. Cells were stained with Lipidtox (H34475, Life Technologies) and LysoTracker Red DND-99 (Life Technologies) at 1:1000 and 1:10,000 respectively for 30 min at room temperature. Pictures were acquired on a Zeiss Axioplan 2 microscope (Zeiss, Jena, Germany) or on a Zeiss LSM 700 confocal microscope.

Transmission electron microscopy

Mice used for transmission electron microscopy analysis of ultrastructure were perfuse-fixed with 3% glutaraldehyde, 1% formaldehyde. Three mice were used for each group. Immunogold staining for cathepsin D was performed on tissue perfuse-fixed with 6% formaldehyde. Anti-cathepsin D was used at 1:200. The secondary rabbit anti-goat IgG 10nm gold (#RAG10, BBI Solutions) was used at a dilution of 1:200.

Thin layer chromatography

Thin layer chromatography (TLC) was performed using standard conditions. Briefly, tissue frozen in liquid nitrogen was powdered and extracted in two changes of chloroform methanol (2:1). Samples were spotted on a TLC plates (1.16487.0001, Merck) and resolved

in hexane:diethyl ether:formic acid (74:25:1). The plate was charred at 100 °C after being sprayed with 10% sulfuric acid. Bands corresponding to free fatty acids, as determined by an oleic acid standard (Sigma), were quantified by using area under the curve analysis in ImageJ software. Amounts of free fatty acid were converted to tissue concentration using the following calculations:

Average micrograms of free fatty acid on TLC plate = 4.79 μg

20 mg of tissue was loaded on each lane of the TLC plate

Therefore, there was 4.79/20 or 0.24 μg per mg of tissue (0.24 μg/mg)

As 1 mg of tissue approximates to 1 μl of volume, 0.24 μg/mg = 0.24 μg/ul

$0.24 \text{ μg/μl} \times 10^6 = 240,000$ μg/l or 0.24 g/l

Oleic acid Mw = 282 g/mol

0.24 g/l / 282 g/mol = 851 μM

Subcellular fractionation of mammary gland tissue

Lymph node dissected number four glands were minced using scalpel blades on ice prior to homogenisation in a tight-fitting handheld homogenizer (12 stokes) in 1 ml of subcellular fractionation buffer (HEPES-KOH 20 mM, sucrose 250 mM, KCl 10 mM, $MgCl_2$ 1.5 mM, EDTA 1 mM, EGTA 1 mM, dithiothreitol 8 mM, Pefabloc 1 mM (Fluka), at pH 7.5). Debris and nuclei were pelleted in a tabletop centrifuge (Heraeus Fresco-17 centrifuge) at 750 g (3,500 r.p.m.) for 10 min, 4 °C. The supernatant was spun at 10,000 g (12,900 r.p.m.) for 15 min at 4 °C, to pellet organelles. The supernatant, containing cytosolic and extracellular components was spun at 100,000 g (40,000 r.p.m.) for 1 h at 4 °C in a BeckmanCoulter Optima L-100 XP Ultracentrifuge to remove microsomes and collected as cytosolic fraction.

Digitonin extraction of EpH4 cells

Cytosolic extraction using digitonin was performed as previously described[59] with the exception that digitonin was used at 25 μg/ml. Briefly, cells were seeded in six-well Nunclon Surface plates (Nunc, 150,000 cells per well) in DMEM, 10% FCS (Gibco/ Sigma) and next day treated with free fatty acids as indicated. Cells were harvested and counted, with 175,000 cells pelleted and extracted with 300 μl of 25 μg/ml Digitonin (300410, Calbiochem) in subcellular fractionation buffer (HEPES-KOH 20mM, sucrose 250 mM, KCl 10 mM, $MgCl_2$ 1.5 mM, EDTA 1 mM, EGTA 1 mM, dithiothreitol 8 mM, Pefabloc 1 mM (Fluka), at pH 7.5), a concentration that had been determined to be optimal (concentrations ranging from 12.5-50 μg/ml were tested and 25 μg/ml showed good cytosolic extraction, with minimal lysosomal damage). Cells were incubated for 10 min on ice with intermittent vortexing. The samples were then spun down (90 s, 13,000 r.p.m., 4 °C) and the supernatant quickly transferred to a new tube to be used in downstream cathepsin activity assays. For each condition 175,000 cells were also extracted in 0.1% TritonX-100 as above to obtain total cell lysates for assessing total cathepsin activity.

Cathepsin activity assay

To measure cytosolic cathepsin activity subcellular fractionation was carried out on mammary glands as described above. Protein levels were assessed with the BCA Protein Assay (Thermo Fisher Scientific, Waltham, MA, USA) and equal amounts of protein (4 μg) were added to a total of 200 μl cathepsin reaction buffer (sodium acetate 50 mM, EDTA 8 mM, dithiothreitol 8 mM and Pefabloc subcellular fractionation buffer 1 mM, at pH 6). Cathepsin B+L activity was measured after incubation (30 min, 37 °C) with the fluorescent substrate Z- Phe-Arg-AMC (50 μM; Merk Millipore, Darmstadt, Germany) in a Synergy HT Multi-Detection Microplate Reader (excitation 380 nM, emission 442 nM; Bio-TEK, Winooski, VT, USA). For assessment of cytosolic cathepsin activity in EpH4 cells treated with free fatty acids 10 μl of digitonin extracted lysates was added to a total of 200 μl cathepsin reaction buffer (sodium acetate 50 mM, EDTA 8 mM, dithiothreitol 8 mM and Pefabloc subcellular fractionation buffer 1 mM, at pH 6) and the fluorescent cathepsin substrate Z- Phe-Arg-AMC (50 μM as above) and fluorescence measured immediately every minute for 1 h at 37 °C (excitation 380 nM, emission 442 nM as above). Initial rates of cathepsin B and L activity were determined from the linear part of the resulting curve and normalised to total cathepsin activity obtained from TritonX-100 extracted lysates.

Lysosomal purification and leakiness assay

Lysosomes from EpH4 cells were purified using magnetic iron nanoparticles (EMG-508, Ferrotec) as previously described[60]. Briefly, EpH4 cells were seeded at a density of 3×10^6 in 15 cm tissue culture plates (168381, Nunc). The following day cells were labelled for 4 h in iron nanoparticle containing media (1:100) followed by a 20 h chase period in clean media. Cells were then scraped off in PBS, pelleted in a tabletop centrifuge (300 r.p.m., 4 °C, 3 min) and the pellet homogenised in a tight-fitting handheld homogenizer (5 stokes) in 700 μl subcellular fractionation buffer (HEPES-KOH 20 mM, sucrose 250 mM, KCl 10 mM, $MgCl_2$ 1.5 mM, EDTA 1 mM, EGTA 1 mM, dithiothreitol 8 mM, Complete protease inhibitor (Roche) at pH 7.5). The homogenate was spun at 750 g (3,500 r.p.m., 4°C, 10 min) to remove nuclei and debri, followed by a second 750 g spin to ensure complete removal of contaminating heavy membranes. The resulting supernatant (pns; post nuclear supernatant) is transferred into a clean tube, loaded onto a magnetic rack and incubated for 1 h at 4 °C on a rocker. A 50 μl sample of pns is retained for analysis. Following incubation tubes are left on the magnet as the supernatant (sn) is removed (retaining 50 μl for analysis). Tubes are washed with 1 ml of subcellular fraction buffer three times. Following addition of last wash tubes are removed and spun at 12,000 r.p.m. (13,800 g, 4 °C, 15 min) to pellet magnetite-containing lysosomes. Pellets were recombined in subcellular fractionation buffer and equal amounts (30μl) aliquoted into individual tubes. Fatty acids (or ethanol control) were added as indicated to a final concentration of 70 μM in a final volume of 60 μl. 70 μM was the lowest concentration of oleic acid that induced reproducible cathepsin leakage. Samples were either re-pelleted immediately (t = 0) at 12,000 r.p.m. (13,800 g, 4 °C, 15 min) or incubated for 30 min (t = 30) at 37°C under gentle agitation. Subsequently, the lysosomes were re-pelleted as above. The supernatant was removed and snap frozen. The pellet was resuspended in 60 μl RIPA buffer (50 mM Tris, 1% NP40, 0.25% sodium deoxycholate, 150 mM NaCl, 1 mM EGTA and complete protease inhibitor), and organelles were lysed on ice for 30 min with intermittent vortexing. Membranes were pelleted at 12,000 r.p.m. (13,800 g,

4 °C, 15 min), the supernatant was removed and equal amounts of the resuspended pellet and the supernatant were analysed by western blot. pns and sn samples were pelleted at 12,000 r.p.m. (13,800 g, 4 °C, 15 min) with the pellet resuspended in 60 μl RIPA buffer and processed similarly to above.

Immunoblotting

Lymph node dissected mammary tissue was snap frozen in liquid nitrogen and ground to a fine powder using a mortar and pestle. Protein from mammary gland powder was extracted in RIPA buffer (50 mM Tris pH 7.4, 1% NP-40, 0.25% sodium deoxycholate, 150 mM NaCl, 1 mM EGTA and 1x Complete protease inhibitor (Roche), 1 mM Na_3VO_4, and 1 mM NaF). Protein concentration was assessed with the BCA Protein Assay (Thermo Fisher Scientific, Waltham, MA, USA) and equal amounts of protein (20 μg) were denatured and resolved on SDS-polyacrylamide gels. Immunoblotting was performed using standard techniques and antibody detection was achieved with enhanced chemiluminescence reagent (ECL, GE Healthcare). The following primary antibodies were used: rat anti-LAMP2 (ab13524, Abcam, 1:1000), goat anti-cathepsin L (AF1515, R&D Systems, 1:1000), mouse anti-COX IV (ab33985, Abcam, 1:1000), goat anti-cathepsin D (AF1029, R&D Systems, 1:1000) and rabbit anti-BTN 1A1 (a generous gift from Dr Ian Mather, 1:5000).

Lysotracker Red staining and flow cytometry

EpH4 cells were seeded on six-well Nunclon™ Surface plates (Nunc, 150,000 cells per well) in DMEM, 10% FCS (Gibco/Sigma). Cells were treated with the indicated concentration of free fatty acids overnight and subsequently harvested and resuspended in 500 μl culture medium. LysoTracker Red DND-99 (Life Technologies, 100 nM) was added to the suspension and incubated at 37 °C in the dark for 30 min. Single-colour flow cytometry was carried out on a CyAn ADP flow cytometer (DakoCytomation), and the data were analysed using the Summit 4.3 software (DakoCytomation).

Quantitative real-time PCR

Lymph node dissected mammary tissue was snap frozen in liquid nitrogen and ground to a fine powder using a mortar and pestle. RNA was extracted from tissue using TRIzol (Life Technologies) according to manufacturer's guidelines. RNA was quantified using a NanoDrop ND-1000 (NanoDrop Technologies) and cDNA synthesised from up to 2 μg of RNA using the SuperScript III First-Strand Synthesis System (Life Technologies) and random hexamers (Life Technologies). SYBR Green JumpStart *Taq*ReadyMix (Sigma) was used for qRT-PCR, with reactions run in a CFX Connect Real Time PCR detection System (BioRad).

Delta Ct values were calculated by subtracting Ct values for Cyclophilin A and relative expression derived using the delta delta Ct method. Primers used were: *cyclophilin A*(housekeeping gene) forward, 5′-CCTTGGGCCGCGTCTCCTT-3′, reverse, 5′-CACCCTGGCACATGAATCCTG-3′; *Btn1a1* forward, 5′-GCCAGGGGAAGGAAGTAGAG-3′, reverse, 5′-ATGGACCCAATGGTGAGAAA-3′; *Xdh* forward, 5′-TGCAGACCCTGAAACAACAC-3′, reverse, 5′-AAGGCGGTCATACTTGGAGA-3′

Data analysis and Statistics

Experimental repeats have been detailed in the figure legends and in Supplementary Table 3. For electron microscopy on animal tissue samples, vesicular fusion events were rare, consistent with their transient nature. In all experiments there were no exclusion criteria, and no data were excluded. All normality and statistical tests were undertaken using GraphPad Prism v4.0a.

Supplementary Material

Refer to Web version on PubMed Central for supplementary material.

Acknowledgements

References

1. Luzio JP, Pryor PR, Bright NA. Lysosomes: fusion and function. Nat Rev Mol Cell Biol. 2007; 8:622–632.

2. Foghsgaard L, et al. Cathepsin B Acts as a Dominant Execution Protease in Tumor Cell Apoptosis Induced by Tumor Necrosis Factor. The Journal of Cell Biology. 2001; 153:999–1010. [PubMed: 11381085]

3. Kroemer G, Jaattela M. Lysosomes and autophagy in cell death control. Nat Rev Cancer. 2005; 5:886–897. [PubMed: 16239905]

4. Cox TM, Cachón-González MB. The cellular pathology of lysosomal diseases. The Journal of pathology. 2012; 226:241–254. [PubMed: 21990005]

5. Manzoni C, Lewis PA. Dysfunction of the autophagy/lysosomal degradation pathway is a shared feature of the genetic synucleinopathies. The FASEB Journal. 2013; 27:3424–3429.

6. Kirkegaard T, Jaattela M. Lysosomal involvement in cell death and cancer. Biochimica et Biophysica Acta (BBA) - Molecular Cell Research. 2009; 1793:746–754. [PubMed: 18948147]

7. Kallunki T, Olsen OD, Jaattela M. Cancer-associated lysosomal changes: friends or foes? Oncogene. 2012; 32:1995–2004. [PubMed: 22777359]

8. Vasiljeva O, et al. Reduced tumour cell proliferation and delayed development of high-grade mammary carcinomas in cathepsin B-deficient mice. Oncogene. 2008; 27:4191–4199. [PubMed: 18345026]

9. Kreuzaler P, Watson CJ. Killing a cancer: what are the alternatives? Nat Rev Cancer. 2012; 12:411–424. [PubMed: 22576162]

10. Watson CJ, Kreuzaler PA. Remodeling mechanisms of the mammary gland during involution. Int J Dev Biol. 2011; 55:757–762.

11. Watson CJ. Involution: apoptosis and tissue remodelling that convert the mammary gland from milk factory to a quiescent organ. Breast Cancer Res. 2006; 8:203. [PubMed: 16677411]

12. Watson CJ, Khaled WT. Mammary development in the embryo and adult: a journey of morphogenesis and commitment. Development. 2008; 135:995–1003. [PubMed: 18296651]

13. Jeong J, et al. A Test of Current Models for the Mechanism of Milk-Lipid Droplet Secretion. Traffic. 2013; 14:974–986. [PubMed: 23738536]

14. Lund LR, et al. Two distinct phases of apoptosis in mammary gland involution: proteinase-independent and -dependent pathways. Development. 1996; 122:181–193. [PubMed: 8565829]

15. Chapman RS, et al. Suppression of epithelial apoptosis and delayed mammary gland involution in mice with a conditional knockout of Stat3. Genes Dev. 1999; 13:2604–2616. [PubMed: 10521404]

16. Humphreys RC, et al. Deletion of Stat3 blocks mammary gland involution and extends functional competence of the secretory epithelium in the absence of lactogenic stimuli. Endocrinology. 2002; 143:3641–3650. [PubMed: 12193580]

17. Kreuzaler PA, et al. Stat3 controls lysosomal-mediated cell death in vivo. Nat Cell Biol. 2011; 13:303–309. [PubMed: 21336304]

18. Kerr JF, Searle J. Deletion of cells by apoptosis during castration-induced involution of the rat prostate. Virchows Arch B Cell Pathol. 1973; 13:87–102. [PubMed: 4201202]

19. Lockshin RA, Zakeri Z. Caspase-independent cell death? Oncogene. 2004; 23:2766–2773. [PubMed: 15077140]

20. Luke CJ, Silverman GA. Necrotic cell death: harnessing the Dark side of the Force in mammary gland involution. Nat Cell Biol. 2011; 13:197–199. [PubMed: 21364568]

21. Aits S, J § §ttel § M. Lysosomal cell death at a glance. Journal of cell science. 2013; 126:1905–1912. [PubMed: 23720375]

22. Galluzzi L, Bravo-San Pedro JM, Kroemer G. Organelle-specific initiation of cell death. Nat Cell Biol. 2014; 16:728–736. [PubMed: 25082195]

23. Kågedal K, et al. Lysosomal membrane permeabilization during apoptosis - involvement of Bax? International Journal of Experimental Pathology. 2005; 86:309–321. [PubMed: 16191103]

24. Ono K, Kim SO, Han J. Susceptibility of Lysosomes to Rupture Is a Determinant for Plasma Membrane Disruption in Tumor Necrosis Factor Alpha-Induced Cell Death. Molecular and Cellular Biology. 2003; 23:665–676. [PubMed: 12509464]

25. Zaragoza R, et al. Nitration of cathepsin D enhances its proteolytic activity during mammary gland remodelling after lactation. Biochem J. 2009; 419:279–288. [PubMed: 19125694]

26. Margaryan NV, et al. New insights into cathepsin D in mammary tissue development and remodeling. Cancer Biology & Therapy. 2010; 10:457–466. [PubMed: 20592493]

27. Helminen HJ, Ericsson JLE. Effects of enforced milk stasis on mammary gland epithelium, with special reference to changes in lysosomes and lysosomal enzymes. Experimental Cell Research. 1971; 68:411–427. [PubMed: 4330916]

28. Gomes LC, Benedetto GD, Scorrano L. During autophagy mitochondria elongate, are spared from degradation and sustain cell viability. Nat Cell Biol. 2011; 13:589–598. [PubMed: 21478857]

29. Klionsky DJ, et al. Guidelines for the use and interpretation of assays for monitoring autophagy. Autophagy. 2012; 8:445–544. [PubMed: 22966490]

30. Mather I, Keenan T. Origin and Secretion of Milk Lipids. J Mammary Gland Biol Neoplasia. 1998; 3:259–273. [PubMed: 10819513]

31. Smith S, Watts R, Dils R. Quantitative gas-liquid chromatographic analysis of rodent milk triglycerides. J. Lipid Research. 1968; 9:52–57. [PubMed: 5688933]

32. Listenberger LL, et al. Triglyceride accumulation protects against fatty acid-induced lipotoxicity. Proceedings of the National Academy of Sciences. 2003; 100:3077–3082.

33. Yuzefovych L, Wilson G, Rachek L. Different effects of oleate vs. palmitate on mitochondrial function, apoptosis, and insulin signaling in L6 skeletal muscle cells: role of oxidative stress. Am. J. Physiol. Endocrinol. Metab. 2010; 299:e1096–1105. [PubMed: 20876761]

34. Huai J, et al. TNF-induced lysosomal membrane permeability (LMP) is downstream of MOMP and triggered by caspase-mediated p75 cleavage and ROS formation. Journal of cell science. 2013; 126:4015–4025. [PubMed: 23788428]

35. Jespersen H, Andersen JH, Ditzel HJ, Mouritsen OG. Lipids, curvature stress, and the action of lipid prodrugs: Free fatty acids and lysolipid enhancement of drug transport across liposomal membranes. Biochimie. 2012; 94:2–10. [PubMed: 21839138]

36. Rammer P, et al. BAMLET Activates a Lysosomal Cell Death Program in Cancer Cells. Molecular Cancer Therapeutics. 2010; 9:24–32. [PubMed: 20053771]

37. Fontana A, Spolaore B, Polverino de Laureto P. The biological activities of protein/oleic acid complexes reside in the fatty acid. Biochimica et Biophysica Acta (BBA) - Proteins and Proteomics. 2013; 1834:1125–1143. [PubMed: 23499846]

38. Ogg SL, Weldon AK, Dobbie L, Smith AJH, Mather IH. Expression of butyrophilin (Btn1a1) in lactating mammary gland is essential for the regulated secretion of milk‚Äìlipid droplets. Proceedings of the National Academy of Sciences of the United States of America. 2004; 101:10084–10089. [PubMed: 15226505]

39. Clarkson R, Wayland M, Lee J, Freeman T, Watson C. Gene expression profiling of mammary gland development reveals putative roles for death receptors and immune mediators in post-lactational regression. Breast Cancer Res. 2004; 6:R92–R109. [PubMed: 14979921]

40. Singh R, et al. Autophagy regulates lipid metabolism. Nature. 2009; 458:1131–1135. [PubMed: 19339967]

41. Monks J, Smith-Steinhart C, Kruk ER, Fadok VA, Henson PM. Epithelial Cells Remove Apoptotic Epithelial Cells During Post-Lactation Involution of the Mouse Mammary Gland. Biology of Reproduction. 2008; 78:586–594. [PubMed: 18057312]

42. Hughes K, Wickenden JA, Allen JE, Watson CJ. Conditional deletion of Stat3 in mammary epithelium impairs the acute phase response and modulates immune cell numbers during post-lactational regression. The Journal of pathology. 2012; 227:106–117. [PubMed: 22081431]

43. Merkel M, Tilkorn A-C, Greten H, Ameis D. Lysosomal Acid Lipase. Methods Mol. Biol. 1999; 109:95–107. [PubMed: 9918015]

44. Atabai K, et al. Mfge8 Is Critical for Mammary Gland Remodeling during Involution. Molecular Biology of the Cell. 2005; 16:5528–5537. [PubMed: 16195353]

45. Hanayama R, Nagata S. Impaired involution of mammary glands in the absence of milk fat globule EGF factor 8. Proceedings of the National Academy of Sciences of the United States of America. 2005; 102:16886–16891.

46. Lockshin RA, Williams CM. Programmed cell death, Cytolytic enzymes in relation to the breakdown of the intersegmental muscles of silkmoths. Journal of Insect Physiology. 1965; 11:831–844. [PubMed: 5828992]

47. Hara-Nishimura I, Hatsugai N. The role of vacuole in plant cell death. Cell Death Differ. 2011; 18:1298–1304. [PubMed: 21637288]

48. van Doorn WG, et al. Morphological classification of plant cell deaths. Cell Death Differ. 2011; 18:1241–1246. [PubMed: 21494263]

49. Cornillon S, et al. Programmed cell death in Dictyostelium. Journal of cell science. 1994; 107:2691–2704. [PubMed: 7876338]

50. Maltese WA, Overmeyer JH. Methuosis: Nonapoptotic Cell Death Associated with Vacuolization of Macropinosome and Endosome Compartments. The American Journal of Pathology. 2014; 184:1630–1642. [PubMed: 24726643]

51. Kitambi SS, et al. Vulnerability of Glioblastoma Cells to Catastrophic Vacuolization and Death Induced by a Small Molecule. Cell. 2014; 157:313–328. [PubMed: 24656405]

52. Unger RH, Scherer PE, Holland WL. Dichotomous roles of leptin and adiponectin as enforcers against lipotoxicity during feast and famine. Molecular Biology of the Cell. 2013; 24:3011–3015. [PubMed: 24072813]

53. Bournazou E, Bromberg J. Targeting the tumor microenvironment: JAK STAT3 signaling. JAK-STAT. 2013; 2:e23828. [PubMed: 24058812]

54. Alonzi T, et al. Essential Role of STAT3 in the Control of the Acute-Phase Response as Revealed by Inducible Gene Activation in the Liver. Molecular and Cellular Biology. 2001; 21:1621–1632. [PubMed: 11238899]

55. Selbert S, Bentley D. Efficient BLG-Cre Mediated Gene Deletion in the Mammary Gland. Transgenic Res. 1998; 7:387–398. [PubMed: 9859227]

56. Roth W, et al. Cathepsin L deficiency as molecular defect of furless: hyperproliferation of keratinocytes and pertubation of hair follicle cycling. The FASEB Journal. 2000; 14:2075–2086. [PubMed: 11023992]

57. Silvestre J-S, et al. Lactadherin promotes VEGF-dependent neovascularization. Nat Med. 2005; 11:499–506. [PubMed: 15834428]

58. Reichmann E, Ball R, Groner B, Friis RR. New mammary epithelial and fibroblastic cell clones in coculture form structures competent to differentiate functionally. The Journal of Cell Biology. 1989; 108:1127–1138. [PubMed: 2466037]

59. Jahreiss L, Renna M, Bittman R, Arthur G, Rubinsztein DC. 1-OHexadecyl-2-O-methyl-3-O-(2′-acetamido-2′-deoxy-beta-D-glucopyranosyl)-sn-glycerol (Gln) induces cell death with more autophagosomes which is autophagy-independent. Autophagy. 2009; 5:835–846. [PubMed: 19550143]

60. Becken U, Jeschke A, Veltman K, Hass A. Cell-free fusion of bacteria-containing phagosomes with endocytic compartments. Proceedings of the National Academy of Sciences. 2010; 107:20726–20731.
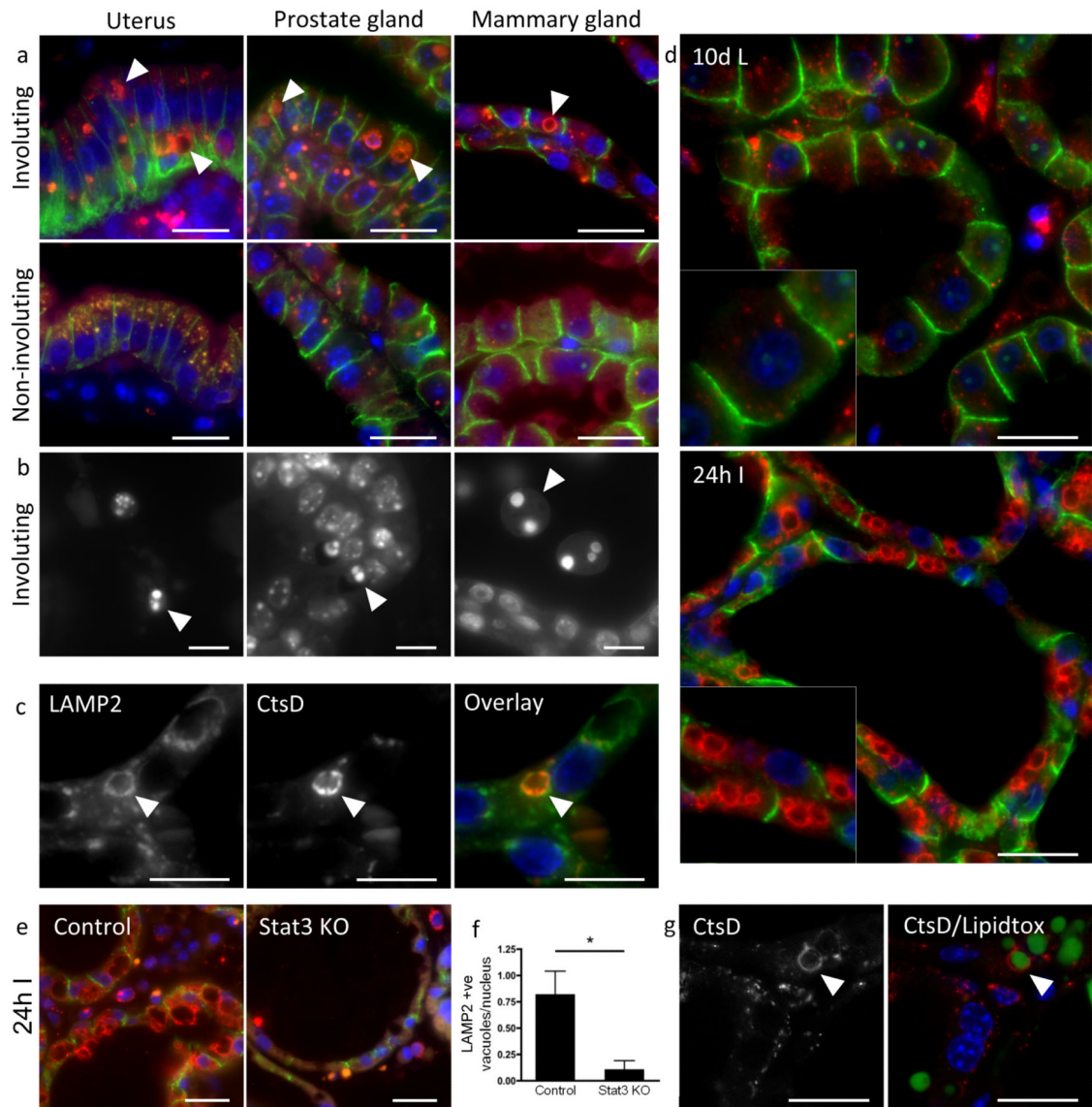
Figure 1.
Enlargement of the lysosomal compartment and digestion of triglyceride in the regressing mammary gland. (a) Large secondary lysosomes are shown by cathepsin D staining (red, arrowheads) in different involuting tissues. Mouse uterus at 24 h post-partum and during late pregnancy, prostate gland at 7 d post castration and uncastrated and mammary gland at 24 h involution and 10 d lactation. Tissue was stained for cathepsin D (red) and E-cadherin (green). (b) Hoescht staining showing dead cells (arrowheads) in the involuting mouse uterus, prostate and mammary gland. Three independent biological repeats per condition for prostate and mammary glands, one biological repeat per condition for uterus. (c) Dual staining for LAMP2 and cathepsin D shows cathepsin D (red) localising to the inside of a LAMP2-positive (green) vacuole. Three independent biological repeats were assessed. (d) LAMP2 (red) and E-cadherin (green) staining in 10 d lactating and 24 h involuting mammary glands. Six independent biological repeats per condition analysed. (e) LAMP2-

positive vacuoles (red) are found in the control but not the Stat3 KO mammary gland at 24 h involution. (f) Staining for LAMP2 at 24 h involution in control and Stat3 knockout animals was quantified. Bars represent means +/− s.e.m. of n = 3 mice per genotype with 12-13 fields counted per mouse (*p<0.05; Student's t-test). Statistics source data can be found in the associated worksheet in Supplementary Table 3 (g) Confocal images showing that cathepsin D-positive vacuoles (arrowhead) contain lipid droplets (lipidtox staining, green) in the 24 h involuting mammary gland. Three independent biological repeats per condition analysed. Nuclei are visualised by Hoescht stain (blue). Scale bars: (a), (d), (e) and (g) = 20 μm, (b) and (c) = 10 μm.
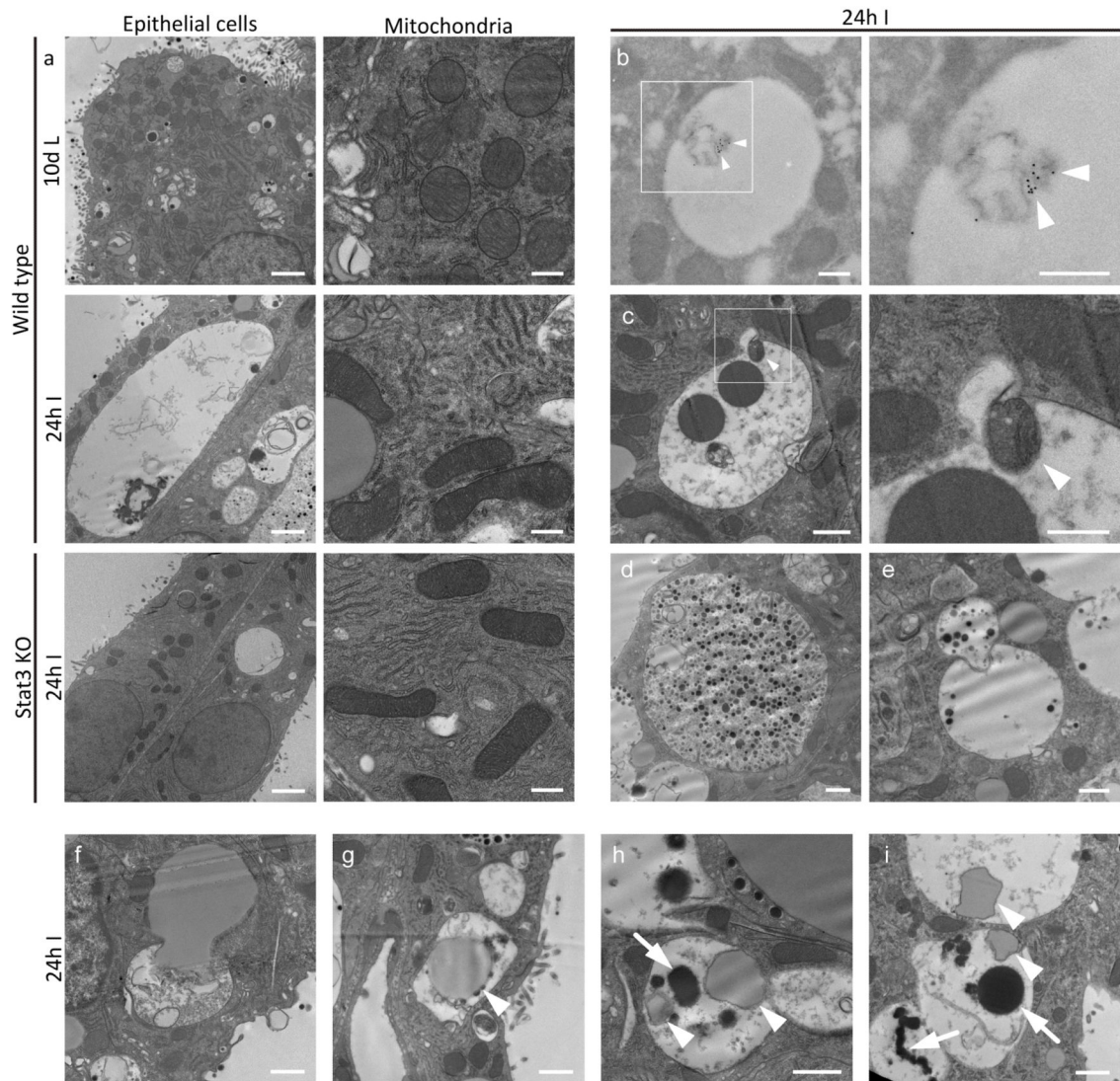
Figure 2.
Ultrastructural analysis of lysosomal vacuoles and cargo delivery. (a) Transmission electron microscopy of wild type 10 d lactation, 24 h involution and Stat3 knockout glands at 24 h involution. (b) Immunogold staining for cathepsin D within large vacuoles at 24 h involution co-localising with degrading material (arrowheads). (c) Autophagic vesicles fusing with large vacuoles (arrowheads), (d) large macropinosomes full of milk inside epithelial cells and milk containing vesicles (e) are seen to fuse with larger vacuoles. (f-i) Membrane bound lipid fuses with vacuoles and can be observed inside lysosomal structures (arrowheads) that contain lipofuscin-like material (arrows). Three animals assessed for all conditions except for cathepsin D-immuno gold staining, where one animal was analysed. Scale bars: (a) epithelial cells = 2 μm, (a) mitochondria, (b) and (c) high magnification = 500 nm, (c) low magnification, (d-i) = 1 μm.
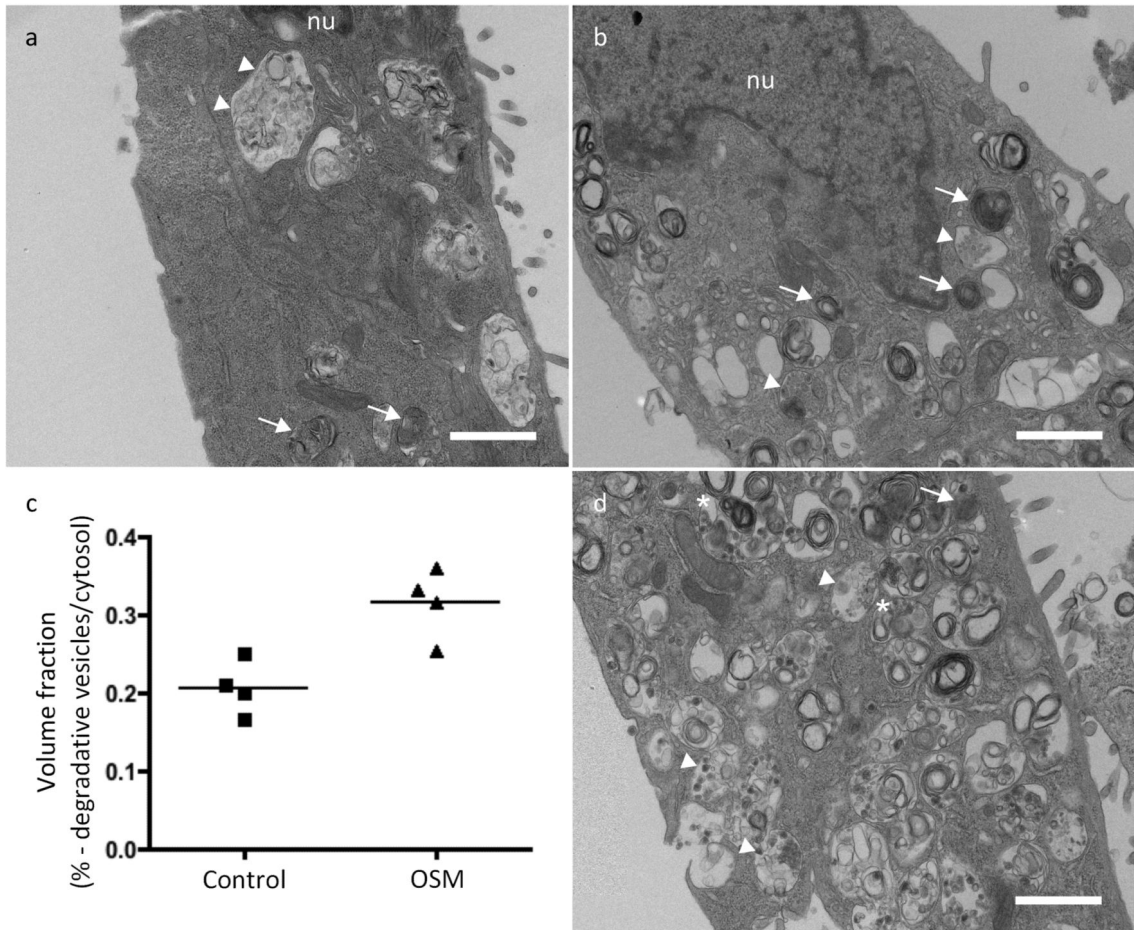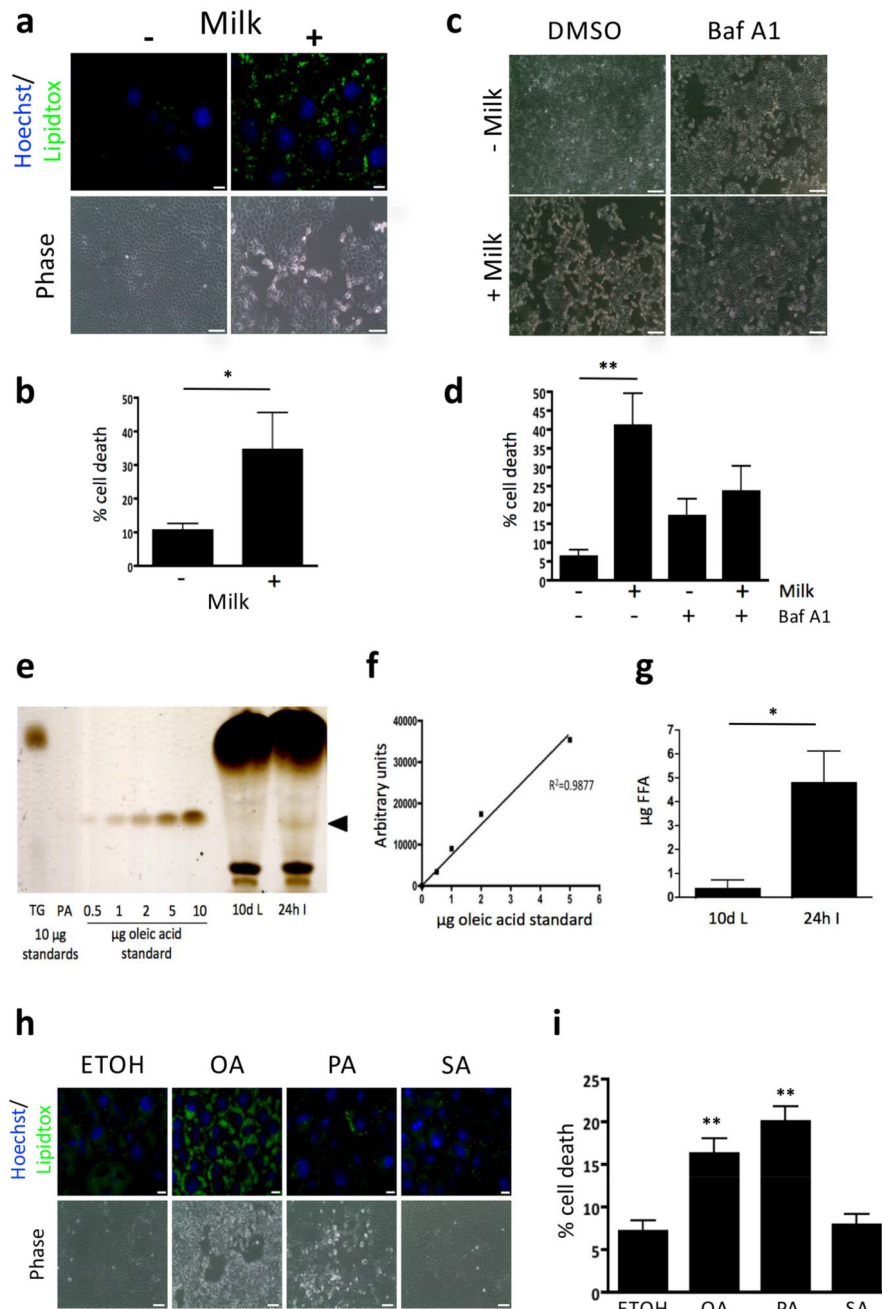
Figure 3.
Vesicular biogenesis in EpH4 cells. (a) Vehicle treated Eph4 cells contain phagosomes/pinosomes (arrowheads) and lysosomes (arrows). (b) EpH4 cells treated with oncostatin M (OSM, 25 ng/ml) for 72 h have 53% more degradative vesicles, as quantified in panel (c) n = 4 individual wells of EpH4 cells seeded on one occasion. Phagolysosomes are marked by an asterisk. (d) In some cases, as a result of oncostatin M treatment, lysosomal vesicles occupied more than half of the cytosolic volume. Scale bars = 1 μm. Statistics source data for Figure 3c can be found in the corresponding worksheet in Supplementary Table 3.

Figure 4.

Free fatty acids are increased during involution and can cause death *in vitro*. (a) Fluorescence and brightfield microscopy shows milk derived lipid accumulation (lipidtox, green) and cell death of EpH4 cells incubated in milk overnight. Scale bars: Lipidtox staining panels =10 μm, phase images = 100 μm. Nuclei are visualised by Hoechst (blue). (b) Milk induced cell death assessed by trypan blue positivity. Means +/− s.e.m. from n=5 independent experiments with 3 technical replicates performed per experiment (*p<0.05; Mann Whitney U test). (c) Bafilomycin A1 treatment partially rescues milk induced cell

death as assessed by brightfield microscopy and trypan blue positivity. (d) Milk induced cell death assessed by trypan blue positivity. Means +/− s.e.m. from n = 4 independent experiments with 3-4 technical replicates performed per experiment (**p<0.01; Kruskal-Wallis test, Dunn's multiple comparison post-test). Scale bars: 250 μm. Cells were pre-treated with Bafilomycin A1 for 1 h prior to milk addition for further 8 h. (e) Thin layer chromatography was used to demonstrate the presence of free fatty acids in mammary gland extracts. Free fatty acids were seen in force involuted mammary gland extracts but not in lactating mammary glands (arrowhead). TG = triglyceride, PA = palmitic acid. (f) A concentration curve of oleic acid is quantified using densitometry. (g) Quantification of the free fatty acid band showed a significant difference between lactating and involuting mammary gland (p<0.05, Student's t-test, n = 4 animals). (h) Fluorescence and brightfield microscopy showing lipid accumulation (lipidtox, green) and cell death of EpH4 cells treated with 500 μM oleic acid (OA), palmitic acid (PA) and stearic acid (SA) overnight. Scale bars: Lipidtox staining panels bars =10 μm, phase images = 100 μm. (i) Fatty acid induced cell death assessed by trypan blue positivity. Means +/− s.e.m. from n = 4 independent experiments with 2-3 technical replicates performed per experiment (**p<0.01 vs ETOH control; one-way ANOVA, Dunnett's Multiple Comparison post-test). Statistics source data can be found in the corresponding worksheets in Supplementary Table 3.
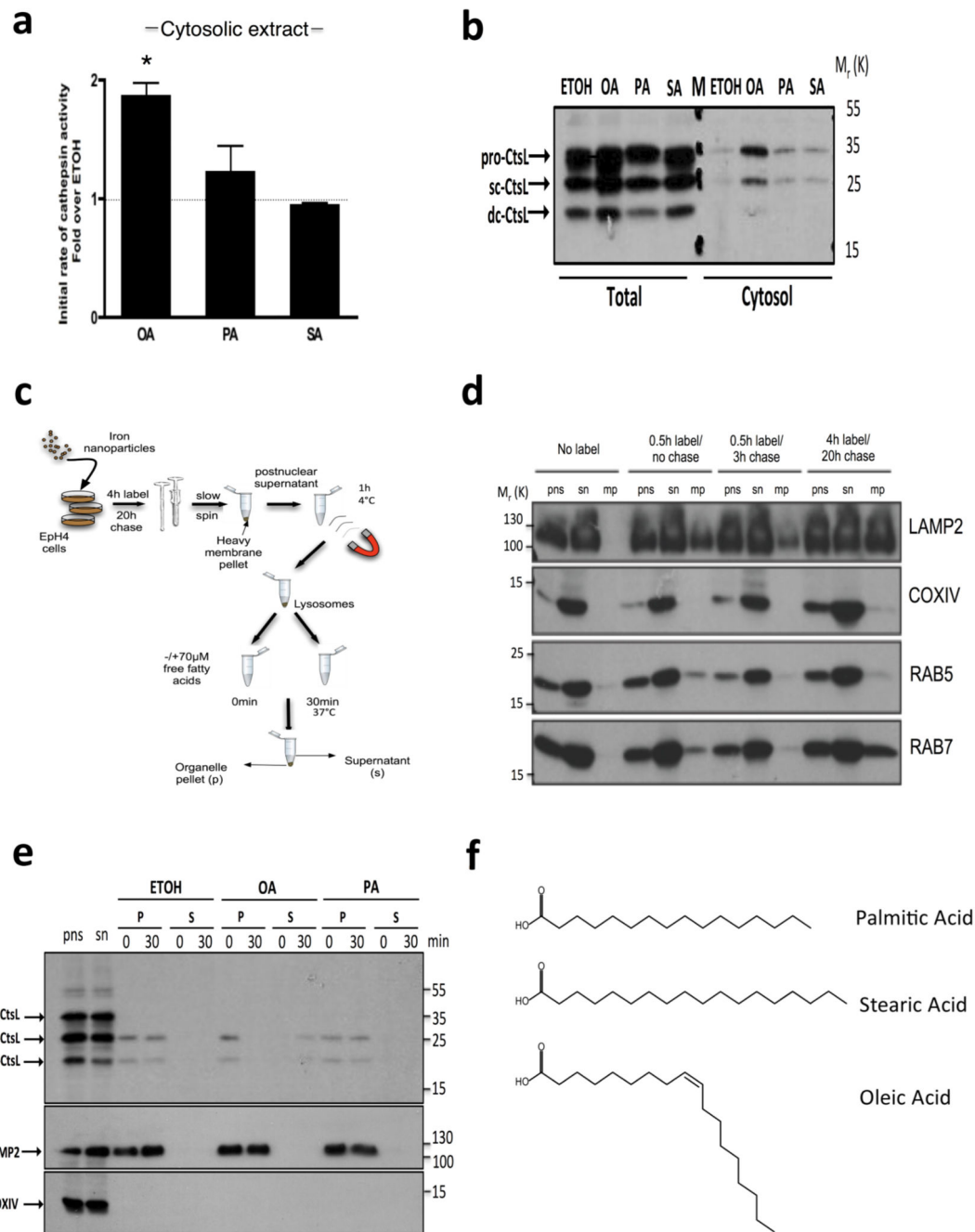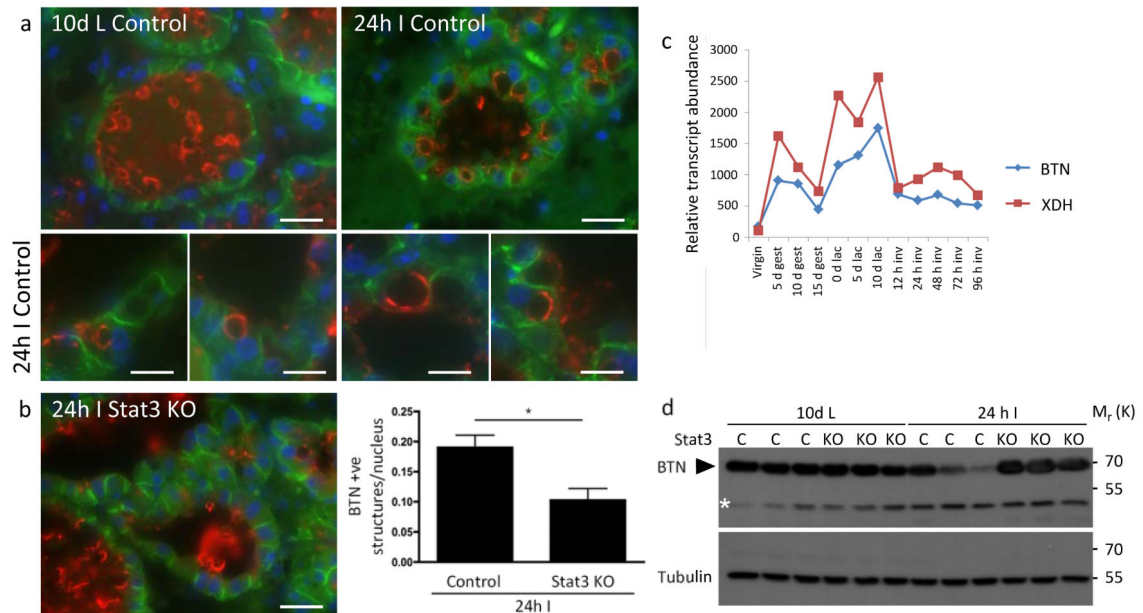
Figure 5.

Free fatty acids induce LMP *in vitro*. (a) Cathepsin activity assay on EpH4 cytosolic extracts treated with 500 μM fatty acids for 16 h demonstrating release of cathepsins to the cytosol by OA. Means +/−s.e.m of n = 4 independent experiments (*p<0.05; Kruskal-Wallis test, Dunn's multiple comparison post-test). (b) Representative sample from (a) was analysed by western blot for Cathepsin L in total and cytosolic EpH4 extracts, showing release of cathepsin L to the cytosol with 500 μM OA. M denotes marker lane. (c) Schematic of iron nanoparticle lysosomal purification protocol. (d) Optimisation of iron nanoparticle mediated

purification of lysosomes from EpH4 cells. Cells were labelled and chased as indicated followed by extraction and immunoblotting. LAMP2, COXIV, RAB5 and RAB7 are shown as markers for lysosomes, mitochondria, early endosomes and late endosomes respectively. Time-course optimisation performed on one occasion. pns; post nuclear supernatant, sn; post magnetic supernatant, mp; magnetic pellet. (e) Cathepsin L immunoblot showing extent of leakiness from the lysosomal pellet (P) into the supernatant (S) at 30 min with 70 μM OA or PA. Representative blot from three independent experiments. LAMP2 was used as a lysosomal marker and COXIV used to show undetectable mitochondrial contamination. (f) Structures of free fatty acids used in this study. Chemical structures for palmitic acid, stearic acid and oleic acid are depicted. Statistics source data can be found in the corresponding worksheet in Supplementary Table 3. Uncropped images of blots appear in supplementary figure 5.

Figure 6.

MFGs are endocytosed by mammary epithelial cells. (a) Staining for MFG membrane protein BTN (red) in 10 d lactating and 24 h involuting mammary gland. (b) Number of butyrophilin-positive structures per nuclei quantified in control and Stat3 knockout 24 h involuting mammary glands. Bars represent means +/− s.e.m. of n = 3 mice per genotype, with 34 alveoli counted per animal (*p<0.05; Student's t-test). Statistics source data can be found in the associated worksheet in Supplementary Table 3. E-cadherin staining is green. Images are representative of three independent biological repeats. (c) Microarray analysis of twelve different timepoints during the mammary gland cycle showing expression of BTN and XDH – "Mammary Gland Pregnancy Cycle Data (.xls)" (http://www.path.cam.ac.uk/~madgroup/microarraysummary.shtml). (d) Western blot for BTN (70 kDa) showing BTN downregulation at 24 h involution in control but not in Stat3 knockout samples. Asterisk indicates a spurious band. Lanes show samples from independent biological repeats. Scale bars: (a) low magnification and (b) = 20 μm, (a) high magnification = 10 μm. Uncropped images of blots appear in supplementary figure 5.
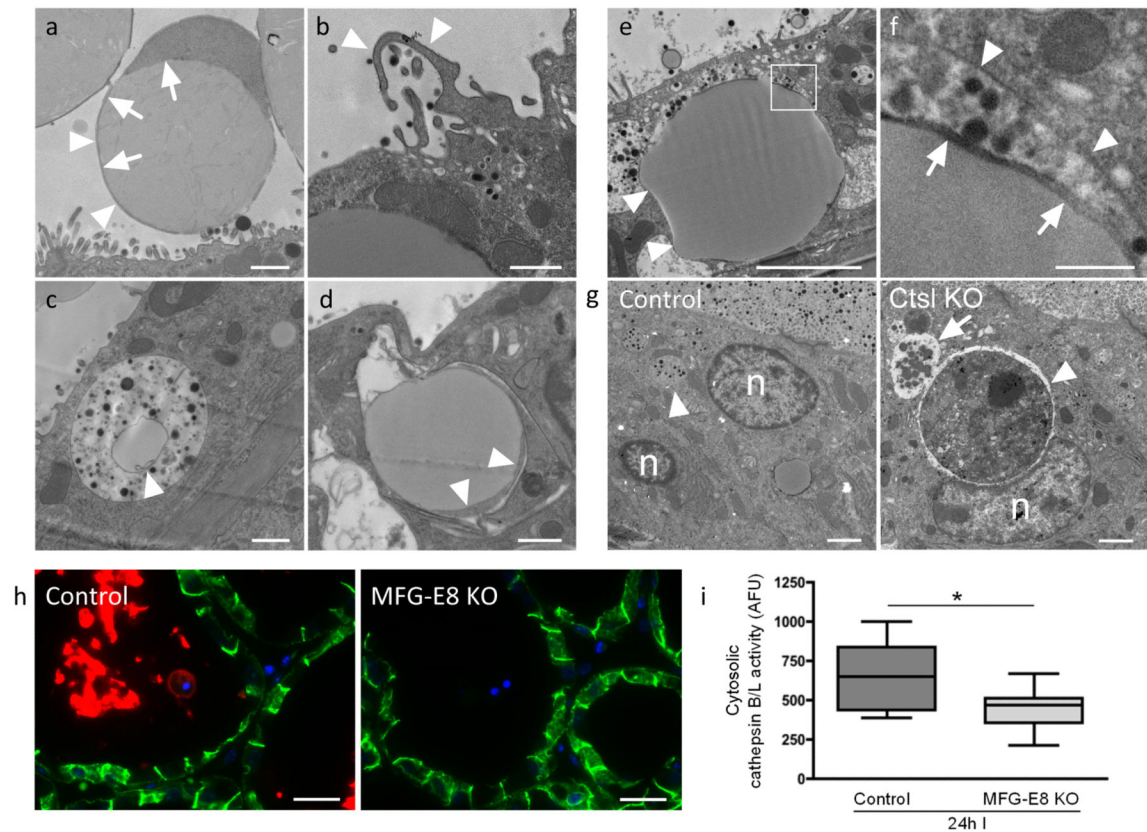
Figure 7.
Uptake of MFGs occurs via macropinocytosis and phagocytosis. (a) MFGs are seen in the alveolar lumen (arrowheads). The cytosolic ring bound by milk fat globule membrane is inherited by the fat droplet as it is secreted through the apical plasmalemma (arrows). (b) Ruffles on the apical plasma membrane are indicative of macropinocytosis (arrowheads). (c) Lipid droplets (arrowhead) are present within milk laden macropinosomes in alveolar epithelium. (d) Phagocytosed milk fat droplets can be identified within epithelium by the presence of MFG associated cytosol and milk fat globule membrane (arrowheads). (e) Another example of a large phagocytosed MFG is shown by arrowheads. The boxed area is enlarged (f) to show the phagosomal membrane (arrowheads) in close apposition to the milk fat globule membrane (arrows). (g) The highly phagocytic nature of alveolar epithelium was demonstrated using cathepsin L KO (Ctsl KO) mice that were force involuted for 72 h. In comparison to wild type controls, cathepsin L KO mammary glands showed accumulation of dead cells within phagosomes (arrowhead). This phagosome is fusing with other vacuoles (arrow). n = nucleus. (h) Staining for the phagocytosis-bridging molecule MFG-E8 (red) and E-cadherin (green) in MFG-E8 heterozygous (control) and knockout mice. Images are representative of three independent biological repeats. (i) Cytosolic cathepsin activity in MFG-E8 control and knockout mice at 24 h involution. Box and whisker plot of n = 12 and n=11 cytoplasmic fractions (mice) for control and knockout groups respectively, with 2 technical replicates performed per fraction (p=0.0173, Student's t-test). Statistics source data can be found in the associated worksheet in Supplementary Table 3. Scale bars: (a)-(d) = 1 μm, (e) = 4 μm and (g) = 2 μm, (f) = 500 nm, (h) = 20 μm.
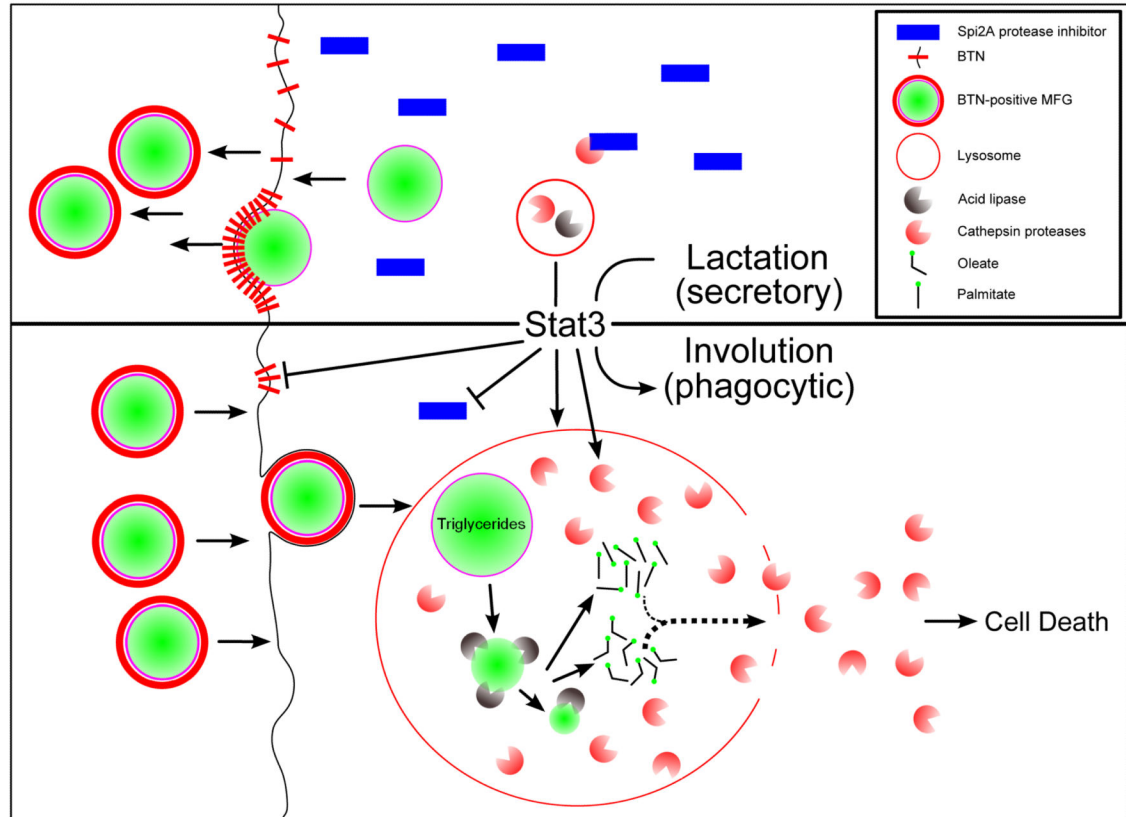
Figure 8.
A schematic model illustrating the role of Stat3 in regulating the transition from a secretory to a phagocytic cell phenotype at the onset of involution. Subsequent cell death ensues due to LMP caused by increase in lysosomal size and generation of free fatty acids from hydrolysis of phagocytosed MFGs within lysosomal vacuoles and leakage of cathepsins into a Spi2a cathepsin inhibitor depleted cytosol.